Novel gold nanoparticles coated with somatostatin as a potential delivery system for targeting somatostatin receptors

Ahmed A. H. Abdellatif, Gamal Zayed, Asmaa El-Bakry, Alaa Zaky, Imran Y. Saleem & Hesham M. Tawfeek

Taylor & Francis
Taylor & Francis Group

RESEARCH ARTICLE

Novel gold nanoparticles coated with somatostatin as a potential delivery system for targeting somatostatin receptors

Ahmed A. H. Abdellatif[a], Gamal Zayed[a], Asmaa El-Bakry[b], Alaa Zaky[b], Imran Y. Saleem[c] and Hesham M. Tawfeek[d]

[a]Department of Pharmaceutics and Industrial Pharmacy, Faculty of Pharmacy, Al-Azhar University, Assiut, Egypt; [b]Department of Pharmaceutics and Industrial Pharmacy, Faculty of Pharmacy, Al-Azhar University, Cairo, Egypt; [c]School of Pharmacy and Biomolecular Science, Liverpool John Moores University, Liverpool, UK; [d]Department of Industrial Pharmacy, Faculty of Pharmacy, Assiut University, Assiut, Egypt

ABSTRACT

Targeting of G-protein coupled receptors (GPCRs) like somatostatin-14 (SST-14) could have a potential interest in delivery of anti-cancer agents to tumor cells. Attachment of SST to different nano-carriers e.g. polymeric nanoparticles is limited due to the difficulty of interaction between SST itself and those nano-carriers. Furthermore, the instability problems associated with the final formulation. Attaching of SST to gold nanoparticles (AuNPs) using the positive and negative charge of SST and citrate-AuNPs could be considered a new technique to get stable non-aggregated AuNPs coated with SST. Different analyses techniques have been performed to proof the principle of coating between AuNPs and SST. Furthermore, cellular uptake studies on HCC-1806, HELA and U-87 cell lines has been investigated to show the ability of AuNPs coated SST to enter the cells via SST receptors. Dynamic light scattering (DLS) indicated a successful coating of SST on the MUA-AuNPs surface. Furthermore, all the performed analysis including DLS, SDS-PAGE and UV-VIS absorption spectra indicated a successful coating of AuNPs with SST. Cellular uptake studies on HCC-1806, HELA and U-87 cell lines showed that the number of AuNPs-SST per cell is signiflcantly higher compared to citrate-AuNPs when quantified using inductively coupled plasma spectroscopy. Moreover, the binding of AuNPs-SST to cells can be suppressed by addition of antagonist, indicating that the binding of AuNPs-SST to cells is due to receptor-specific binding. In conclusion, AuNPs could be attached to SST via adsorption to get stable AuNPs coated SST. This new formulation has a potential to target SST receptors localized in many normal and tumor cells.

Introduction

Gold nanoparticles (AuNPs) are considered to be very important and applicable tool in nanotechnology. This is due to their easy surface functionalization and/or bio-conjugation, stability and biocompatibility. They have been the subjects of many studies and many applications in medicine and in biology, such as immunoassays, drug targeting of cancer cells and in biomedical research[1,2]. AuNPs were delivered to ovarian cancer cells that express the epidermal growth factor receptor and the folate receptor, the ovarian cell took all particles by active transport[3]. It was found that tumor cells can be killed by excitation of internalized AuNPs, the internalized AuNPs were excited by laser beam which killed the cancer cells[4].

SSTRs are members of the G-protein coupled receptors (GPCRs) super family[5,6]. There are five different subtypes of SSTRs (SSTR$_{1-5}$), SSTR$_2$ having been classified into two subtypes, SSTR$_{2A}$ and SSTR$_{2B}$[7,8]. The blocking of SSTRs with antagonist suppresses the interaction of the peptide agonist with SSTRs[9]. SSTRs are present in the surface of numerous normal and diseased cells; they are expressed in normal tissues such as the pituitary gland and pancreas[8,10]. SSTRs are also expressed in many tumor cells i.e. small cell and non-small lung cancer[11–13], neuroendocrine tumors and breast cancer[14], colorectal carcinoma, gastric cancer and hepatocellular carcinoma[15]. SSTR$_2$ is expressed in glucagonoma 1, glucagonoma 2[16], metastatic lymph nodes[17], insulinoma 1 & 2 and 3[16,18–20], normal adrenal gland and pheochromocytoma types 1 & 2 and 3[21]. It is also found that the majority of human cancer cells (benign or malignant), are over express SSTRs[22]. They are often characterized by the changing their surface receptors[23]. Targeting of SST receptors could be beneficial in SST receptor-expressing tumors; hence targeting of specific molecules e.g. peptides-ligand SST-to-SST receptors in vivo is a successful method to treat various types of cancers. The SST receptors subtypes belong to a superfamily of G protein-coupled receptors that can functionally couple to various intracellular effector system[24]. Different systems and pass ways have been extensively studied and documented for the action of SST receptors in tumor e.g. the adenylcyclase cAMP-protein kinase a pathway that can be inhibited by SST in numerous cell types and the modulation of potassium channels by SST[6]. Other relevant signaling pathways regulated by SST include the SST induced stimulation of phospholipase A2[25] and the activation of phosphotyrosine phosphatases[26]. In addition, the expression of SST receptors was highly variable from one individual to another and from one tumor type to another. Whereas some tumors are characterized by a high density of receptors, such as meningiomas or medulloblastomas, others, such as lymphomas, have a much lower density. Some tumors have a rather homogeneous SSTRs distribution, e.g. most neuroendocrine tumors, in particular gastroenteropancreatic tumors. Other tumors, such as breast carcinomas, are characterized, however, by a highly heterogeneous SSTRs distribution, with regions of high density next to regions lacking the receptor[27]. Hence, SSTRs could be considered a promising target for normal and diseased cells using nanoparticulate delivery

systems, reducing side effects and increasing the drug concentration in the tumor[28].

Receptor-mediated endocytosis is an important example of a specific internalization mechanism following ligand binding to their receptor[29–31]. It allows for an import of extracellular molecules for around 1000-fold increase of the intracellular concentration of macromolecules[32–34]. In the process of endocytosis, the plasma membrane is engulfed inwards from specialized membrane microdomains forming either clathrin or caveolin-coated pits[34].

The limited stability and the presence of many functional groups within SST make the interaction with other compounds such as PEGylation with thiolated-PEG is difficult[35]. Many trials have been performed in our laboratory for PEGylation of SST or even attaching any other polymer to coat AuNPs. Such trials showed the difficulty of such attachment due to the numerous functional groups of SST. Moreover, it may affect the structure and integrity of SST.

Up to date and according to our research in literature, we have the first attempt to rationally develop and formulate a novel stable non-aggregated AuNPs coated with SST. AuNPs coated with SST system has a potential to active target SST receptors for diagnostic as well as therapeutic purposes. The novel prepared system utilizing the absorption between the positively charged SST and the negatively charged citrate-AuNPs at neutral pH. AuNPs were prepared by citrate reduction method and coated with 11-MUA to facilitate the binding with SST. Furthermore, the stability and the ability to adsorb SST to either citrate-coated-AuNPs or 11-MUA-coated AuNPs were investigated. The prepared citrate-AuNPs, MUA-AuNPs and AuNPs coated with different concentrations of SST were examined for their size, polydispersity and surface charge. Moreover, the dissociation and adsorption of SST to AuNPs were also studied and confirmed using sodium dodecyl sulfate and polyacrylamide gel electrophoresis. Cellular uptake study for citrate-AuNPs, AuNPs-SST and AuNPs-SST together with antagonist was also performed using HCC-1806, HELA and U-87 cell lines. In addition, the amounts of Au internalized into the cells were quantified using inductively coupled plasma spectroscopy (ICP-OES).

Materials and methods

Materials

Somatostatin-14 acetate (SST-14) was kindly supplied from CuraMED Pharma GmbH (Karlsruhe, Germany). Hydrogen tetrachloroaurate trihydrate, 11-Mercaptoundecanoic acid (11-MUA), RPMI 1640 medium, bovine serum albumen, chloroauric acid (HAuCl$_4$) and cyn-154806 trifluoroacetate (TFA) were purchased from Sigma Aldrich (Steinheim, Germany). Tri-sodium citrate dihydrate, sodium chloride, sodium hydroxide, nitric acid, hydrochloric acid, triethylamine, sodium dihydrogen phosphate, disodium hydrogen phosphate were purchased from Merck (Darmstadt, Germany). Dulbecco's phosphate buffered saline (pH 7.4), Dulbecco's Modified Eagle Medium and Leibovitzs L-15 were purchased from Invitrogen (Paisley, UK). Triple negative breast cancers cells (HCC-1806) were kindly supplied from Dr. Abdellatif Bouazzaoui (Haematology and Internal Oncology, Regensburg University, Germany). The purified water used for all experiment was obtained using a Milli-Q water purification system from Millipore (Schwalbach, Germany). Human adenocarcinoma (Hela cells) and Human gliobastoma (U-87) were purchased from ATCC Co, Egypt. Any other chemicals and solvents were of analytical grade.

Preparation of AuNPs capped with SST-14

Preparation of citrate-AuNPs

First, citrate-AuNPs were prepared according to a previously reported procedure[36–38]. Briefly, 3 mL of 38.8 mM tri-sodium citrate solution were added to 100 mL of 0.3 mM chloroauric acid (HAuCl$_4$) solution in a 250 mL round bottom flask. The reaction mixture stirred vigorously and heated under reflux. Refluxing was continued for 15 min, and then the prepared AuNPs was left to cool at room temperature[38]. Stirring was continued for an additional 15 min. AuNPs were purified from larger aggregates by centrifugation for 30 min at 2450×g using an Avanti centrifuge J-E/Beckman coulter GmbH, Germany.

Stabilization of the synthesized citrate-AuNPs

The 11-MUA was deposited on the gold surface to facilitate the electrostatic binding between SST-14 and AuNPs[39–41]. Briefly, 1 mL of 1 mM stock solution of 11-MUA was added to 20 mL of the prepared AuNPs solution in a 100 mL Erlenmeyer flask. After adjusting the pH to 11, the AuNPs were incubated with 11-MUA under continuous stirring at 600 rpm at room temperature overnight. This allows sufficient exchange of citrate anions with 11-MUA on the particle surface. The stabilized particles were purified by centrifugation at 15 700×g for 20 min in a falcon tube using an Avanti centrifuge J-E/Beckman coulter GmbH, Germany. The supernatant was decanted and the precipitate was resuspended again in 1 mL Millipore water[40].

Coating of MUA-AuNPs with SST

First, different concentrations of SST (20, 40, 60, 100 and 200 nM) were studied to show the optimal concentration for coating. In brief, 3 mL of the prepared MUA-AuNPs were mixed with 100 μL of 10 mM NaCl as isotonic solution and stirred for 30 min[42]. Then the stabilized MUA-AuNPs were added drop-wise to 10 μL of different concentrations of SST-14 to determine the optimum concentration of SST-14 that can load to AuNPs. The solution was stirred for another 30 min. The stabilized AuNPs-SST was purified by centrifugation at 15 700×g for 15 min, using (Eppendorf centrifuge 5415R, Hamburg, Germany), the supernatant was decanted and the precipitate was re-suspended again in Millipore water. The steps of deposition and purifications are shows in Figure 1.

Characterization of AuNPs capped with SST

Size and surface charge

To determine the size, count rate and zeta potential of AuNPs, the samples were adjusted to 25 ± 1.0 °C and laser light scattering analysis was performed with an incident laser beam of 633 nm at a scattering angle of 90° using the Malvern zetasizer nano 6.01 (Malvern Instruments GmbH, Herrenberg, Germany). The sampling time was set automatically. Moreover, three measurements were allowed to perform each 10 sub-runs and, all measurements were carried out in aqueous solution. The results were calculated from the average of three independent measurements[38].

Dissociation of SST from AuNPs-SST by solid sodium dodecyl sulfate

Sodium dodecyl sulfate (SDS) was used to adsorb and dissociate the AuNPs from the formulated AuNPs-SST leaving SST free in solution. Then, the free SST was quantified using HPLC. In brief, 3 mL of the purified AuNPs-SST were incubated with 3 mg solid SDS at room temperature and left overnight. SDS adsorbed the AuNPs
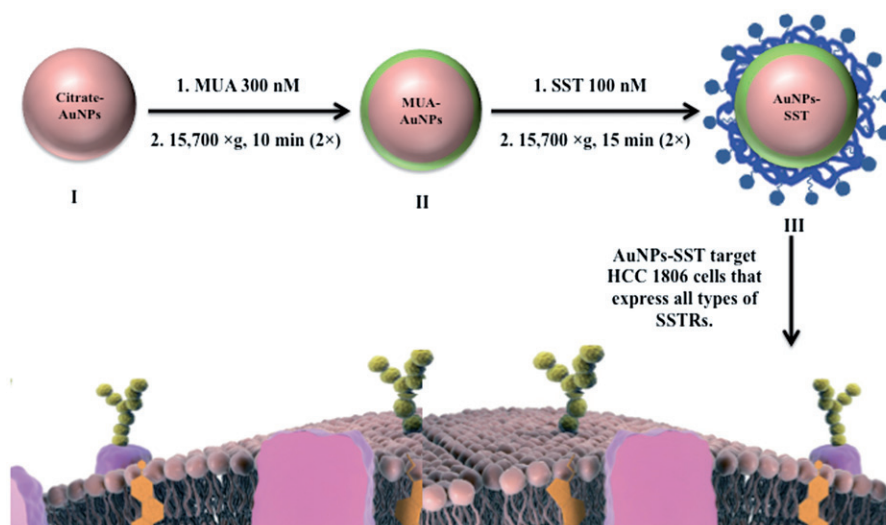
Figure 1. Schematic diagram for deposition of SST onto MUA-AuNPs. 10 mM of NaCl used as isotonic solution. MUA-AuNPs was added drop-wise to 10 μL of concentration of 100 nM SST stirred for 30 min and purified by centrifugation at 15 700×g for 15 min.

from AuNPs-SST leaving SST-14 free in the supernatant which it can be measured and identified by HPLC.

HPLC analysis was performed for SST-14 using a system with a Degasser (Knauer, Berlin, Germany), LC-10AT pump (SpectraLab Scientific Inc., Markham, Canada), FCV-10ATVP gradient mixer (Bio Surplus, San Diego, MA), SIL-10ADVP autosampler (McKinley Scientific, Sparta, NJ), CTO-6A column oven (Varian Inc., Mississauga, ON, Canada), SPD-10AV UV-detector (Gen Tech Scientific, Mill Street Arcade, NY), RF-551 fluorescence detector (Shimadzu, Duisburg, Germany) and SCL-10AVP controller (Shimadzu, Duisburg, Germany). HPLC analysis was performed for SST using linear gradient method from 26% to 39% acetonitrile in water, with 0. 1% TFA, as mobile phase was applied over 15 min at a flow rate of 1.0 mL/min. The samples were separated at a temperature of 40 °C using a C18-reversed Precolumn (LC 318, 4.6 mM ×5.0 mm). Chromatograms were detected by UV detection at 210 nm and 274 nm[43].

Identification of the attached SST to AuNPs using sodium dodecyl sulfate

Polyacrylamide gel electrophoresis
The adsorbed SST to AuNPs was determined using SDS-PAGE as previously reported[44,45]. In brief, 21 μL of AuNPs-SST was mixed with 7 μL modified SDS-PAGE sample buffer. Without heating, the samples were loaded in duplicates onto a 6% SDS-PAGE gel. Then, the normal gel running procedure was followed. Putamol was used to over fill the separating gel. Electrophoresis was run in a constant mode at 100 mA using Pharmacia Biotech Electrophoresis Power Supply EPS (Bridge Path Scientific, 4841 International Boulevard, Frederick, MD). It was running on discontinuous buffer system. The running was also using separating gels (6%) and collecting gel (1.2 mL acrylimide, 2 mL collecting gel buffer, 5 μL TEMED and 80 μL APS 10%). Then 10 μL of protein ladder of 19, 26, 34, 48, 85 or 117 kDa were used as control protein. Gels were stained by Coomassie Brilliant Blue G-25 dispersion.

UV–VIS spectroscopy of AuNPs and AuNP-SST
UV–VIS absorption spectra of the citrate-AuNPs, MUA-AuNPs and AuNPs decorated with SST were recorded using an Uvikon 941 UV–VIS absorbance spectrophotometer (Kontron Instruments GmbH). It was taken five spectra of each gold colloid suspension in the range from 400 to700 nm. The absorbance measurements were made using 0.5 cm path length quartz cuvettes. The SPR is clearly visible as a peak in the range between 514 and 550 nm.

Cellular uptake study
HCC-1806, HELA and U-87 cell lines were used to study the cellular uptake of SST-decorated AuNPs. HCC-1806 and HELA cells express all types of SSTRs. U-87 cells were taken as negative control as they weakly expresses SSTRs. SSTRs expression was confirmed and tested in our lab as reported previously[38,46,47]. HCC-1806 expression of SSTRs was confirmed by Reverse Transcription Polymerase Chain Reaction (RT-PCR)[48]. Cells were cultured in T-75 tissue culture flasks in RPMI 1640 supplemented with 10% FCS[49].

Cellular uptake study of AuNPs-SST using inductively coupled plasma-optical

Emission spectroscopy ICP-OES
To determine quantitatively the number of AuNPs entered per cell, all the used cells were incubated for 1 h at 37 °C with 1 mL of 100 nM of citrate-AuNPs and AuNPs-SST. The incubation was performed in 1 mL of serum-containing culture medium with serum free Leibowitz medium in T-75 tissue culture flasks. To displace the bound AuNPs-SST, the cells were incubated prior to the experiment for 20 min with 100 μL of 1 mM antagonist (cyn-164806). The AuNPs concentrations were determined in 96-well plate using an Uvikon 941 UV–VIS absorbance spectrophotometer (Kontron Instruments GmbH)[50]. To harvest cells, 2 mL of trypsin-EDTA was added to the flask. The flasks were incubated at 37 ± 0.5 °C for 3 min to allow cell detachment. The cells were washed with DPBS two times, followed by centrifugation at 300×g (18 ± 0.5 °C) for 5 min in order to pellet the cells. The cells were transferred to a 5 mL glass vials.

ICP-OES sample preparation and determination of AuNPs
This technique is specifically used to determine the concentration of Au^{3+} metals, minor and major concentrations as a previously reported[40,51]. Typically, 500 μL of each sample containing AuNPs was mixed with 200 μL of freshly prepared aqua regia then diluted

to 5 mL with Millipore water. The Au^{3+} content of the digested cells was determined using ICP-OES on a JY-70 PLUS (Jobin Yvon Instruments S.A.). The plasma flow was 16 mL/min argon. Concentrations of 1, 10 and 100 ppm were used as a standard concentration of gold (III) chloride. The numbers of AuNPs per cell were determined by ICP-OES (for details of calculation refer the Supplemental data).

Statistical analysis

Cellular uptake study was subjected to statistical analysis using one-way analysis of variance (ANOVA). Minitab® 16 Statistical Software (Minitab, Ltd., Brandon, UK) with the Tukey's multiple comparison was employed for comparing the formulations with each other. Statistically significant differences were assumed when $p \leq 0.05$.

Results and discussion

Preparation and characterization of AuNPs

Citrate coated AuNPs were synthesized as reported previously[40]. During this synthesis, a color change was observed when tri-sodium citrate was added to $HAuCl_4$ solution. The solution was initially of yellowish color. After the citrate was added, the color changed first to light blue, dark blue, then purple, dark purple and finally red to purple in color (Figure 2).

The obtained series of color change indicated the formation of small and uniform citrate-AuNPs via the citrate-reduction method using a molar ratio of 3:1 tri-sodium citrate to $HAuCl_4$. Furthermore, the formulated citrate-AuNPs were uniform in particle size of 19.3 ± 0.5 nm and had a negative surface charge of -43.4 ± 0.5 mV (Figure 3).

Size (hydrodynamic diameter), Polydispersity index (PDI) and zeta potential of particles are parameters that indicate the stability of nanoparticles[52,53]. High PDI indicates the heterogeneity of the particle size in suspension. While smaller PDI values indicate the homogeneity of the particle size in suspension. It was reported that PDI lower than 0.2 is considered to be ideal hence, the particle size distribution falls within a narrow range of size[52,54–57]. The surface charge also plays an important role in the stability of the nanoparticles and the magnitude of zeta potential is indicative of the colloidal stability of the system[58].

In addition, the mean count rate and PDI were monitored (Figure 3). The high-count rate 185 kpcs, indicated that the concentration of nanoparticles was high enough for measurements. Furthermore, the PDI was very small 0.16, indicating that the colloidal AuNPs were uniform and has a very narrow size distribution range.

Stabilization of the synthesized AuNPs using 11-MUA

A stronger stabilizing agent, 11-MUA, was used instead of citrate to achieve successful coating of AuNPs with SST-14. 11-MUA is a thiol compound that binds strongly to gold surfaces. Citrate-AuNPs were coated with 11-MUA at pH 11. The carboxyl group of 11-MUA is deprotonated at pH 11 and can stabilize the particle dispersion via electrostatic repulsion[42]. After coating of AuNPs with 11-MUA, the size increased to 23.5 ± 0.05 nm with a PDI of about 0.2 (Figure 4). After the purification of MUA-AuNPs, the PDI decreased to a value of 0.1 indicating that the free 11-MUA was removed from the colloidal solution, and MUA-AuNPs turned to a more stable and more monodisperse colloidal solution.

It was found that the zeta potential was highly negative, -73.2 ± 0.06 mV for crude MUA-AuNPs. After purification, the zeta
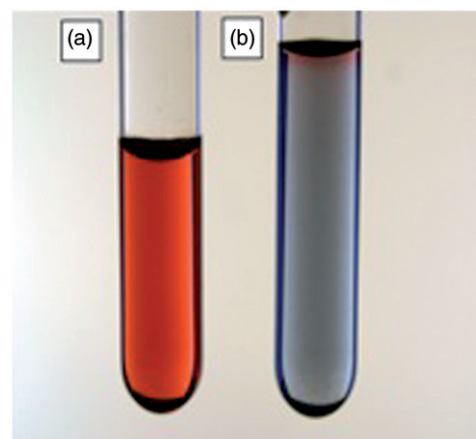

Figure 2. Image of (a) monodispersed AuNPs with red to purple color, (b) polydispersed aggregated AuNPs with a blue color. (Please refer to the online version for the colored image.)
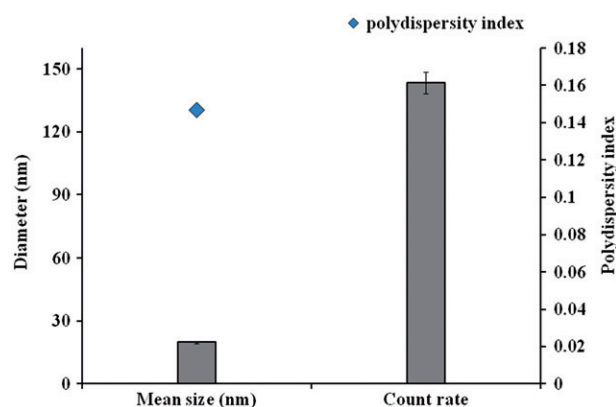

Figure 3. Particle size distribution, count rate as well as the polydispersity index (Diamond) of citrate-AuNPs of 19 nm using DLS.
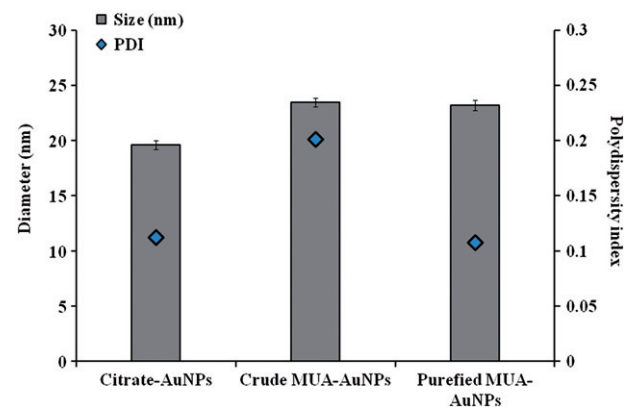

Figure 4. The hydrodynamic diameter as well as PDI of citrate-AuNPs, crude MUA-AuNPs and purified MUA-AuNPs.

potential increased to become less negative, -65.3 ± 0.1 mV, but still high enough to stabilize the particles in an aqueous environment (Figure 5). On the same time, this highly negative charge is ideal for an adsorptive immobilization of SST-14.

Influence of different ionic strength on the stability of MUA-AuNPs

Ionic strength is very important for the stability of colloidal nanoparticles[59]. In addition, ionic strength is considered one of the most important factors that influence the adhesion of a molecule
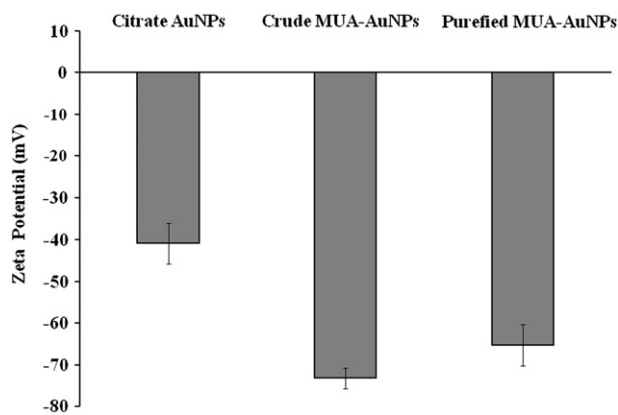
Figure 5. Zeta potential of citrate-AuNPs, crude MUA-AuNPs and purified MUA-AuNPs as a function of stability.
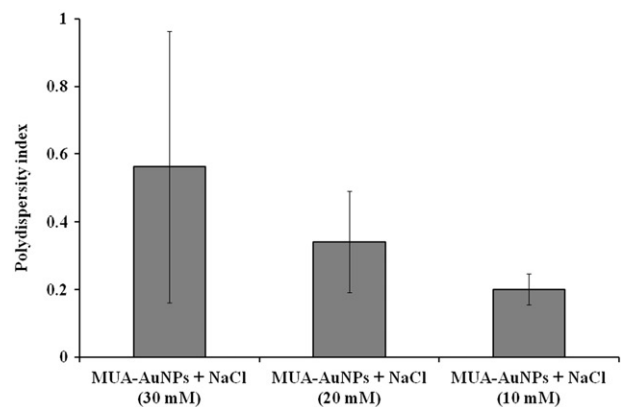

Figure 6. Influence of ionic strength on the polydispersity index of 11-MUA coated AuNPs. The PDI of MUA-AuNPs with 10 mM NaCl is satisfactory low. In contrast, the PDI with 20 and 30 mM NaCl were much higher, which indicate the beginning of aggregation.
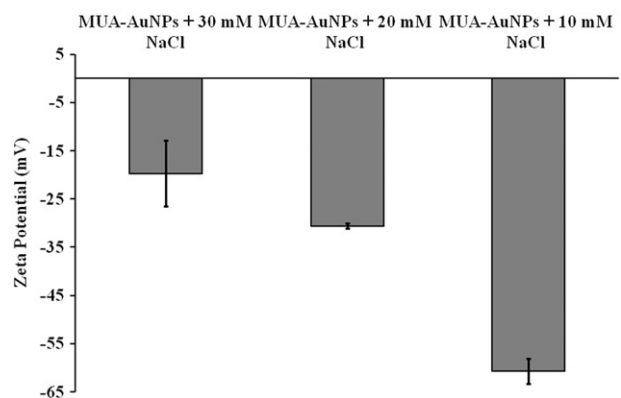
to nanoparticles surfaces[40]. To determine the ideal ionic strength, different concentrations of NaCl (10, 20 and 30 mM) were tried to choose the optimum concentration which stabilize the coating of MUA-AuNPs with SST-14. Furthermore, the stability of the particles at different ionic strengths was determined by monitoring the change in the particles size, zeta potential and PDI. A concentration of 10 mM NaCl proved to be a suitable ionic strength for maintaining a small hydrodynamic diameter and low PDI of MUA-AuNPs during the coating and puriflcation processes. On the other hand, MUA-AuNPs with 20 and 30 mM NaCl, showed aggregation with undefined particle sizes. The PDI of MUA-AuNPs of 10 mM NaCl was 0.2 ± 0.04. In contrast, the PDI for 20 and 30 mM NaCl was 0.34 ± 0.8 and 0.5 ± 0.3, respectively (Figure 6) which indicated the beginning of particle aggregation and instability. This could be attributed to the increase in PDI in these higher molar concentrations. It was found that increasing the ionic strength led to a decrease in the Debye length between the particles concomitant with particles aggregation[60].

Zeta potential analysis was performed for identification of the change in the surface charge of MUA-AuNPs at different ionic strengths (Figure 7). The MUA-AuNPs mixed with 100 μL of 10 mM NaCl had a high negative surface charge of -60.7 ± 2.1 owing to the presence of carboxylate anions from 11-MUA. Increasing the ionic strength to 20 and 30 mM, decreased the negative surface potential to a value of -20.6 ± 0.5 and -19.7 ± 6.8 mV, respectively, leading to the aggregation of the nanoparticles (Figure 7). This was accompanied by a color change from red to blue as depicted (Figure 2). This interaction is most likely due to increased Van der Waals forces[58,61–63]. From the above results, it was clear that AuNPs are reasonably stable after 11-MUA coating and resist the aggregation in the presence of up to 10 mM NaCl.

Figure 7. Zeta potential measurements of MUA-AuNPs at different ionic strength 10, 20 and 30 mM NaCl. The MUA-AuNPs mixed with 10 mM NaCl had a high negative surface charge. Increasing the ionic strength to 20 and 30 mM, decreased the negative surface potential, leading to aggregation of the nanoparticles. This was accompanied by a color change from red to blue.

Table 1. Particle size by intensity (percentage), polydispersity index as well as zeta potential of AuNPs coated with different concentrations of SST.

Parameters	SST concentration (nM)	Size (nm)	PDI	Zeta potential (mV)
Citrate-AuNPs	0	18.2 ± 0.2	0.14	-40.93 ± 4.8
MUA-AuNPs	0	20.2 ± 0.1	0.12	-60.63 ± 2.6
AuNPs-SST	20	21.7 ± 0.1	0.2	-46.8 ± 2.6
AuNPs-SST	40	22.5 ± 0.3	0.1	-22.7 ± 1.9
AuNPs-SST	60	23.5 ± 0.2	0.2	16.9 ± 2.9
AuNPs-SST	100	25.1 ± 0.1	0.1	20.3 ± 1.3
AuNPs-SST	200	28.3 ± 0.4	0.2	29.3 ± 1.3

Coating of MUA-AuNPs with SST-14

The coating process of SST-14 on MUA-AUNPs could be performed according to the adsorption between oppositely charged groups. SST-14, which has a positive charge, was adsorbed on a negatively charged MUA-AuNPs. However, at neutral pH somatostatin (SST-14) homing two lysine residues, is positively charged twice, these positive charges make SST easier to adsorb on MUA-AuNPs. Different concentrations of SST-14 were tried to choose the best and high-adsorbed amounts of SST-14. The amount of SST-14 adsorbed to AuNPs seemed to increase from 20 to 200 nM. The particle sizes increased to 21.7 ± 0.06, 22.4 ± 0.3, 23.5 ± 0.2, 25.05 ± 0.07 and 28.3 ± 0.4 for different SST-14 concentrations of 20, 40, 60, 100 and 200 nM, respectively with acceptable PDI (Table 1). After

purification, the nanoparticles were stable without aggregation. However, particles coated with a concentration of 200 nM SST-14 showed aggregates after 6 h, indicating that they are not acceptable preparations for a long-term stability. For that reason, the ideal SST-14 concentration to be used for coating was chosen to be 100 nM because the formed particles were stable in size and did not form aggregates.

Therefore, zeta potential was measured to confirm the successful coating of AuNPs with SST-14. Citrate-AuNPs had a zeta potential of -40.9 ± 4.9 mV. After deposition of 11-MUA, it became more negative, -60.8 ± 2.65 mV, indicating that citrate was replaced with 11-MUA and the surface of gold coated carboxylic acid groups. Moreover, the zeta potential of all the investigated particles was initially negative then, after coating with different concentrations of 20–200 nM SST-14, it became less negative. Furthermore, AuNPs-SST-14 at 60, 100 and 200 nM showed a reversal of the zeta

potential values from negative to positive (16.9, 20.3 and 29.3 mV, respectively, Table 1). Thus, zeta potential study proved the successful loading of SST-14 on the surface of MUA-AuNPs.

The significance of 11-MUA for coating of SST-AuNPs

Since the citrate-AuNPs have a negative surface charge and SST-14 has a positive charge. SST-14 might be deposited on the surface of AuNPs without of 11-MUA as an intermediate coating. To investigate this aspect, AuNPs were mixed with SST-14 solution directly. The results of this experiment showed that 11-MUA is essential for coating of SST-14 to AuNPs. Since, the absence of 11-MUA during the coating of citrate-AuNPs with SST-14 led to an aggregation of AuNPs. Accordingly, the deposition of SST-14 on MUA-AuNPs showed no aggregation even at higher concentration of SST-14 about 100 nM (Figure 8a). While citrate-AuNPs formed aggregates after all purification steps even it was coated with 20 nM of SST-14 (Figure 8b).

Hence, it was worthy to use 11-MUA for coating of SST-14 to AuNPs, since it make the AuNPs more stable and can adsorb easily SST-14. Furthermore, the aggregation observed in citrate-AuNPs could be possibly attributed to the failure of SST-14 to replace the citrate anion on the surface of AuNPs which may formed as positive negative complex or could be the disulfide bond of SST-14 was reduced by citrate that make the particles aggregated.

Dissociation of AuNPs-SST by sodium dodecyl sulfate (SDS)

The effects of ionic surfactants like SDS on AuNPs-SST were studied using HPLC. At pH 7.0, anionic surfactants such as SDS induce peptide dissociation for AuNPs-SST. For this reason, SDS was used to confirm the adsorption of SST-14 to AuNPs. Figure 9 shows the chromatograms of SST-14 and SST-14 dissociated from AuNPs-SST-14. The dissociation of SST-14 from AuNPs showed a single peak eluted at about 3.6 min. The chromatogram showed no degradation products. The SST-14 dissociated from AuNPs was eluted earlier than the free SST-14, because it was less hydrophilic due to

the presence of some traces of 11-MUA. Thus, confirmed the adsorption of SST-14 to AuNPs, which then dissociated from the AuNPs with SDS.

SST-14 adsorbed to the surface of AuNPs was also analyzed using SDS-PAGE. Figure 10 shows the SDS-PAGE containing a single band for AuNPs-SST-14 (lane 5) that does not move. This confirmed the attachment of SST-14 to the AuNPs which hinder the peptide from moving in the applied electric field[64,65]. On the other hand, the 100 nM concentration of SST-14 and citrate-AuNPs showed no bands (lane 3 and lane 4, respectively). However, increasing the concentration of SST-14 to 100 nM resulted in appearance of band (lane 2) which is also confirmed the attachment of SST-14 to AuNPs.

UV-VIS spectroscopy of AuNPs and AuNPs decorated with SST-14

The optical properties of AuNPs are highly dependent on the nanoparticle diameter. Smaller nanoparticles absorb light and have peaks near 520 nm, while larger spheres exhibit increased scattering and have peaks shifted toward longer wavelengths (known as red-shift). Furthermore, larger spheres scatter more light because they have larger optical cross sections, and their albedo (a ratio of
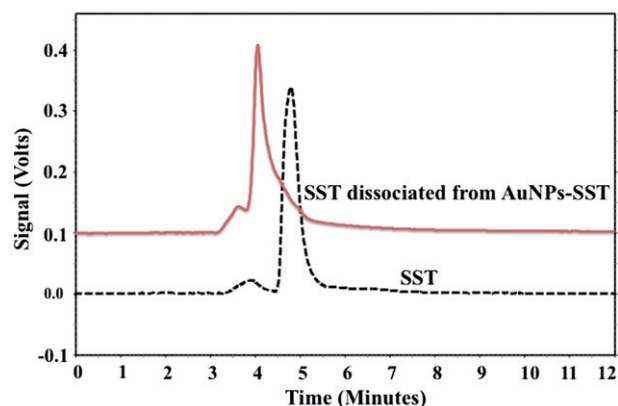

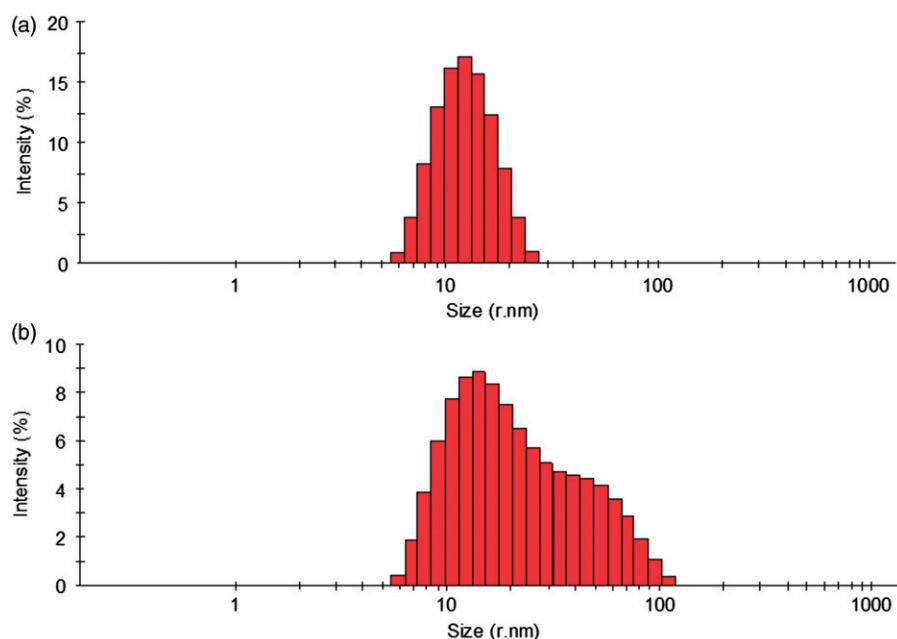Figure 9. HPLC chromatograms of SST dissociated from AuNPs-SST using SDS.

Figure 8. Particle size distribution of AuNPs measured using DLS. (a). Coated with SST at concentration of 100 nM after deposition on MUA-AuNPs using 10 mM NaCl as polyelectrolyte. (b). Coated directly with SST at concentration of 20 nM after deposition directly on citrate-AuNPs without using 10 mM NaCl as polyelectrolyte.

scattering to total extinction) increases with size. AuNPs are often used as bio-imaging tags in dark field microscopy techniques, where the scattering from individual nanoparticles with diameters larger than 40–50 nm can be observed[40]. The UV–VIS spectra of citrate-AuNPs, MUA-AuNPs and AuNPs-SST showed a small red shift in the surface plasmon resonance peak. The shifts observed were of values of 5 and 4 nm for, SPR, MUA-AuNPs and AuNPs-SST-14, respectively (Figure 11). This could be possibly attributed to the deposition of 11-MUA and SST-14 on AuNPs and increasing the nanoparticles size.

Cellular uptake study

To study the cellular uptake of AuNPs-SST, HCC-1806, HELA and U-87 cells were chosen as a model cell lines. Cells were incubated with citrate-AuNPs (as control nanoparticles) and AuNPs-SST for 1 h in RPMI 1640 medium containing serum. The investigated cell lines
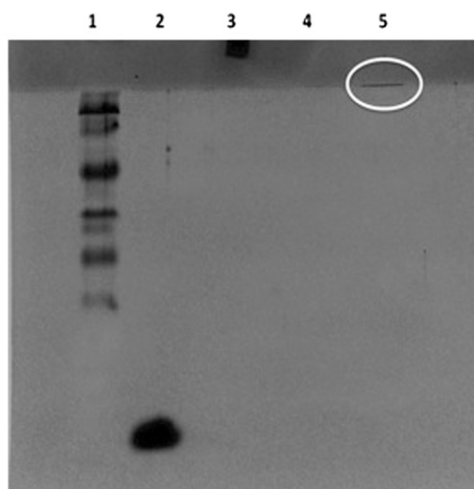

Figure 10. SDS-PAGE analysis for identification of the attachment of SST to AuNPs using 20% acrylamide, and protein ladder 19 KDa. For identification of SST, a protein ladder was used (lane 1). High concentration of SST (10 mM) (lane 2), 100 nM SST (lane 3), citrate-AuNPs (lane 4) and 200 nM AuNPs decorated with SST (lane 5).

took up all types of AuNPs and the average amount of AuNPs per cell strongly depended on the presence or absence of SST receptors. Since all kinds of AuNPs are of nearly similar sizes but possess different outer layers, this suggests that surface properties may strongly affect interactions with the cells. The number of AuNPs per cell was determined by ICP-OES. The initial concentration of AuNPs in the culture medium was 100 nM for citrate-AuNPs, MUA-AuNPs and AuNPs-SST. AuNPs-SST were internalized in significantly ($p < 0.05$; ANOVA/Tukey) higher amounts (estimated number, 15393 ± 656 per cell) more than citrate-AuNPs and AuNPs-SST (estimated number 3779 ± 758 and 8649 ± 570 per cell, respectively) in the presence of the antagonist (cyn 154806) (Figure 12). However, the higher amounts of antagonist up to 1 mM displaced the nanoparticles from the receptor. Hence, it can be concluded that the difference in the cellular uptake of AuNPs-SST is due to differences in surface properties and not in the size of AuNPs. Nanoparticle interaction with cells is an issue of importance for targeting of these particles to different cells. These results counteract the evidence of unwanted interactions such that particles enter cells with a nonspecific way when they are exposed to colloids. SST-14 as SSTRs agonist could easily fit on the SSTRs which increase the internalization of AuNPs, whilst blocking of these receptors by antagonist like cyn-154806 led to internalization of AuNPs.

ICP-OES showed also a higher binding of AuNPs-SST to HELA cells while a weak binding for AuNPs-SST to U-87 cells. Additionally, these results with HELA and U-87 cells match the results reported previously by Abdellatif et al.[38,46,47] Since, the higher binding of AuNPs-SST with HELA cells could be attributed to higher expression of mRNA of SSTR2, while lower expression of mRNA has a lower binding with AuNPs-SST. Moreover, these results showed that the internalization binding was reduced in the presence of free antagonist cyn-164806. On other word, the internalization of AuNPs-SST was significantly decreased when displaced with free antagonist cyn-164806, due to blocking of receptors.

Conclusions

Citrate-AuNPs were efficiently synthesized via the citrate-reduction method. They are uniform in size 19.3 ± 0.5 nm and had a negative
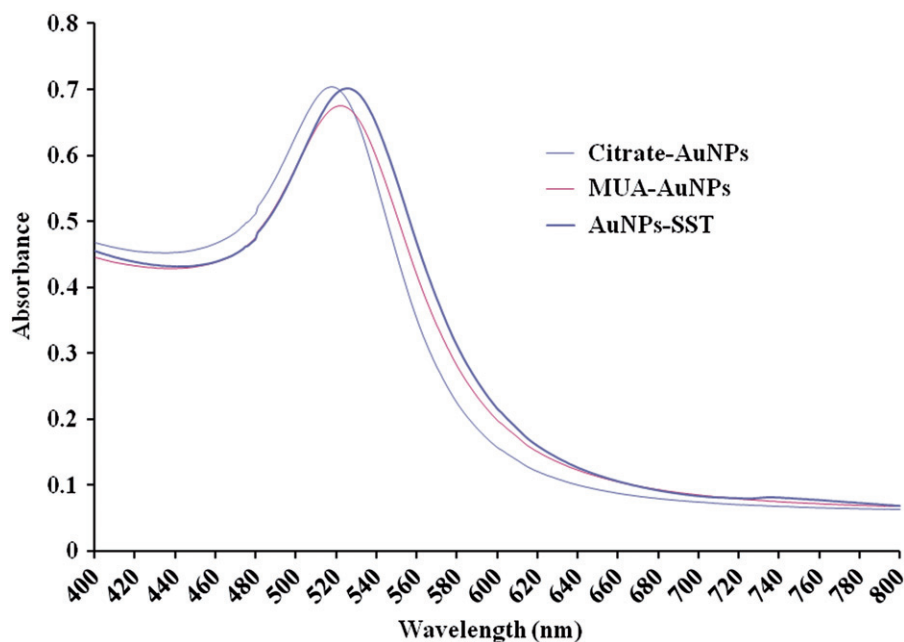

Figure 11. UV–VIS spectra of AuNPs, from top to bottom: citrate-AuNPs, purified AuNPs capped 11-MUA, and purified AuNPs decorated with SST.
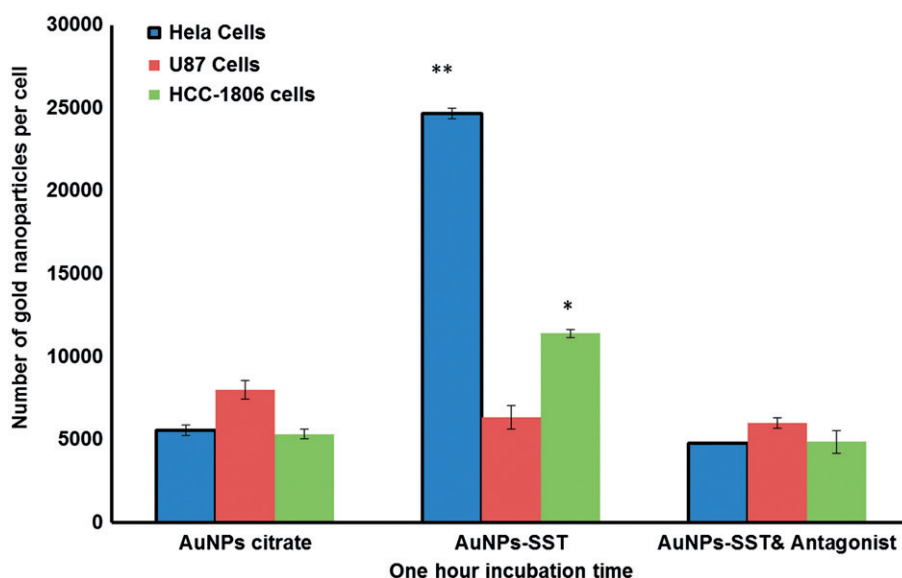
Figure 12. The cellular uptake of AuNPs as determined by ICP-OES and cell counting after 1 h of incubation. The concentration of AuNPs in the culture medium was 100 nM for citrate-AuNPs, and AuNPs-SST. *Significantly different ($p \leq 0.05$; ANOVA/Tukey) versus citrate-AuNPs and AuNPS-SST (100 nM +1 ml antagonist) in HCC-1806 cells. **Significantly different ($p \leq 0.05$; ANOVA/Tukey) versus citrate-AuNPs, AuNPS-SST (100 nM +10 μM antagonist) in HELA cells compared with HCC-1806 (positive control cells) and U-87 (negative control cells).

charge of -43.4 ± 0.5 mV. Moreover, AuNPs were stable, resist the aggregation and successfully coated with SST-14 after binding with 11-MUA instead of citrate ions. All analytical tools used in our study e.g. DLS, SDS-PAGE and UV–VIS absorption spectra confirmed the attachment of SST-14 to AuNPs. In addition, significantly ($p < 0.05$; ANOVA/Tukey) higher amounts AuNPs-SST particles internalized per cell in HCC-1806 and HELA cell lines compared to citrate-AuNPs and AuNPs-SST in the presence of antagonists. Such internalization depends on the surface properties of the cells not on the size of particles as shown when the receptors were blocked by incorporation of antagonist. Finally, the proof of principle has been addressed and we will focusing our research in the future in the delivery of these novel AuNPs coated with SST-14 to various tumor cells.

Disclosure statement

Funding information

References

1. Huang KJ, Li J, Liu YM, et al. Disposable immunoassay for hepatitis B surface antigen based on a graphene paste electrode functionalized with gold nanoparticles and a Nafion-cysteine conjugate. Microchim Acta 2012;177:419–26.
2. Saleh M, Soliman H, Haenen O, El-Matbouli M. Antibody-coated gold nanoparticles immunoassay for direct detection of Aeromonas salmonicida in fish tissues. J Fish Dis 2011; 34:845–52.
3. Bhattacharyya S, Khan JA, Curran GL, et al. Efficient delivery of gold nanoparticles by dual receptor targeting. Adv Mater 2011;23:5034–8.
4. Kang B, Mackey MA, El-Sayed MA. Nuclear targeting of gold nanoparticles in cancer cells induces DNA damage, causing cytokinesis arrest and apoptosis. J Am Chem Soc 2010; 132:1517–19.
5. Hoyer D, Bell GI, Berelowitz M, et al. Classification and nomenclature of somatostatin receptors. Trends Pharmacol Sci 1995;86–8.
6. Patel YC. Somatostatin and its receptor family. Front Neuroendocrinol 1999;20:157–98.
7. Rufini V, Calcagni ML, Baum RP. Imaging of neuroendocrine tumors. Semin Nucl Med 2006;36:228–47.
8. Taniyama Y, Suzuki T, Mikami Y, et al. Systemic distribution of somatostatin receptor subtypes in human: an immunohistochemical study. Endocr J 2005;52:605–11.
9. Long JB. Spinal subarachnoid injection of somatostatin causes neurological deficits and neuronal injury in rats. Eur J Pharmacol 1988;149:287–96.
10. Reubi JC, Waser B, Schaer JC, Laissue JA. Somatostatin receptor sst1-sst5 expression in normal and neoplastic human tissues using receptor autoradiography with subtype-selective ligands. Eur J Nucl Med 2001;28:836–46.
11. Rivera JA, Alturaihi H, Kumar U. Differential regulation of somatostatin receptors 1 and 2 mRNA and protein expression by tamoxifen and estradiol in breast cancer cells. J Carcinog 2005;4:10.
12. Virgolini I, Traub T, Novotny C, et al. Experience with indium-111 and yttrium-90-labeled somatostatin analogs. Curr Pharm Des 2002;8:1781–807.
13. Weiner RE, Thakur ML. Radiolabeled peptides in oncology: role in diagnosis and treatment. BioDrugs 2005;19:145–63.
14. Sharma K, Srikant CB. Induction of wild-type p53, Bax, and acidic endonuclease during somatostatin-signaled apoptosis in MCF-7 human breast cancer cells. Int J Cancer 1998;76:259–66.
15. Reynaert H, Rombouts K, Vandermonde A, et al. Expression of somatostatin receptors in normal and cirrhotic human liver and in hepatocellular carcinoma. Gut 2004;53:1180–9.

16. Nowak KW, Strowski MZ, Switonska MM, et al. Evidence that orexins A and B stimulate insulin secretion from rat pancreatic islets via both receptor subtypes. Int J Mol Med 2005;15:969–72.

17. Behr TM, Gratz S, Markus PM, et al. Enhanced bilateral somatostatin receptor expression in mediastinal lymph nodes ("chimney sign") in occult metastatic medullary thyroid cancer: a typical site of tumour manifestation? Eur J Nucl Med 1997;24:184–91.

18. Roosterman D, Brune NEI, Kreuzer OJ, et al. Intracellular degradation of somatostatin-14 following somatostatin-receptor 3-mediated endocytosis in rat insulinoma cells. Febs J 2008;275:4728–39.

19. Wente W, Efanov AM, Treinies I, et al. The PDZ/coiled-coil domain containing protein PIST modulates insulin secretion in MIN6 insulinoma cells by interacting with somatostatin receptor subtype 5. Febs Let 2005;579:6305–10.

20. Roosterman D, Glassmeier G, Baumeister H, et al. A somatostatin receptor 1 selective ligand inhibits Ca2+ currents in rat insulinoma 1046-38 cells. Febs Let 1998;425:137–40.

21. Kubota A, Yamada Y, Kagimoto S, et al. Identification of somatostatin receptor subtypes and an implication for the efficacy of somatostatin analogue SMS 201-995 in treatment of human endocrine tumors. J Clin Invest 1994;93:1321–5.

22. Patel YC. Molecular pharmacology of somatostatin receptor subtypes. J Endocrinol Invest 1997;20:348–67.

23. McMahon KA, Zajicek H, Li WP, et al. SRBC/cavin-3 is a caveolin adapter protein that regulates caveolae function. Embo J 2009;28:1001–15.

24. Reubi JC. Peptide receptors as molecular targets for cancer diagnosis and therapy. Endocr Rev 2003;24:389–427.

25. Schweitzer P, Madamba S, Siggins GR. Arachidonic acid metabolites as mediators of somatostatin-induced increase of neuronal M-current. Nature 1990;346:464–7.

26. Colas B, Cambillau C, Buscail L, et al. Stimulation of a membrane tyrosine phosphatase activity by somatostatin analogues in rat pancreatic acinar cells. Eur J Biochem 1992;207:1017–24.

27. Reubi J, Waser B, Foekens J, et al. Somatostatin receptor incidence and distribution in breast cancer using receptor autoradiography: relationship to EGF receptors. Int J Cancer 1990;46:416–20.

28. Nilsson O, Kolby L, Wangberg B, et al. Comparative studies on the expression of somatostatin receptor subtypes, outcome of octreotide scintigraphy and response to octreotide treatment in patients with carcinoid tumours. Br J Cancer 1998;77:632–7.

29. Zhang D, Lee HF, Pettit SC, et al. Characterization of transferrin receptor-mediated endocytosis and cellular iron delivery of recombinant human serum transferrin from rice (Oryza sativa L.). BMC Biotechnol 2012;12:92.

30. Thomsen LB, Lichota J, Larsen TE, et al. Brain delivery systems via mechanism independent of receptor-mediated endocytosisi and adsorptive mediated endocytosis. Curr Pharm Biotechnol 2012;13:2349–54.

31. Wang H, Wu L, Reinhard BM. Scavenger receptor mediated endocytosis of silver nanoparticles into J774A.1 macrophages is heterogeneous. ACS Nano 2012;6:7122–32.

32. Delehanty JB, Mattoussi H, Medintz IL. Delivering quantum dots into cells: strategies, progress and remaining issues. Anal Bioanal Chem 2009;393:1091–105.

33. Chen B, Liu QL, Zhang YL, et al. Transmembrane delivery of the cell-penetrating peptide conjugated semiconductor quantum dots. Langmuir 2008;24:11866–71.

34. Kelf TA, Sreenivasan VKA, Sun J, et al. Non-specific cellular uptake of surface-functionalized quantum dots. Nanotechnology 2010;21:28.

35. Herrmann J, Bodmeier R. Degradation kinetics of somatostatin in aqueous solution. Drug Dev Ind Pharm 2003;29:1027–33.

36. Kimling J, Maier M, Okenve B, et al. Turkevich method for gold nanoparticle synthesis revisited. J Phys Chem B 2006;110:15700–7.

37. Frens G. Controlled nucleation for regulation of particle-size in monodisperse gold suspensions. Nat Phys Sci 1973;241:20–2.

38. Abdellatif AAH, Rasoul SAE, Osman S. Gold nanoparticles decorated with octreotide for somatostatin receptors targeting. J Pharm Sci & Res 2015;7:14–20.

39. Bhattacharjee RR, Mandal TK. Polymer-mediated chain-like self-assembly of functionalized gold nanoparticles. J Colloid Interface Sci 2007;307:288–95.

40. Elbakry A, Zaky A, Liebkl R, et al. Layer-by-layer assembled gold nanoparticles for siRNA delivery. Nano Lett 2009;9:2059–64.

41. Chang CW, Chu SP, Tseng WL. Selective extraction of melamine using 11-mercaptoundecanoic acid-capped gold nanoparticles followed by capillary electrophoresis. J Chromatogr A 2010;1217:7800–6.

42. Lin SY, Tsai YT, Chen CC, et al. Two-step functionalization of neutral and positively charged thiols onto citrate-stabilized Au nanoparticles. J Phys Chem B 2004;108:2134–9.

43. Brizzi V, Corradini D. Rapid analysis of somatostatin in pharmaceutical preparations by HPLC with a micropellicular reversed-phase column. J Pharmaceut Biomed 1994;12:821–4.

44. Khalkhali-Ellis Z. An improved SDS-polyacrylamide gel electrophoresis for resolution of peptides in the range of 3.5-200kDa. Prep Biochem 1995;25:1–9.

45. Brandl F, Hammer N, Blunk T, et al. Biodegradable hydrogels for time-controlled release of tethered peptides or proteins. Biomacromolecules 2010;11:496–504.

46. Abdellatif AAH, et, al. Targeting of somatostatin receptors using quantum dots nanoparticles decorated with octreotide. J Nanomed Nanotechnol 2015;6:2.

47. Abdellatif AAH, et, al. Octreotide labelled fluorescein isothiocyanate for identification of somatostatin receptor subtype 2. Biochem Physiol 2015;4:2.

48. Seitz S, Schally AV, Gluck S, et al. Effective treatment of triple-negative breast cancer with targeted cytotoxic somatostatin analogue AN-162 (AEZS-124). J Clin Oncol 2009;27:15.

49. Keller PJ, Lin A, Arendt LM, et al. Mapping the cellular and molecular heterogeneity of normal and malignant breast tissues and cultured cell lines. Breast Cancer Res 2010;12:R87.

50. Haiss W, Thanh NT, Aveyard J, Fernig DG. Determination of size and concentration of gold nanoparticles from UV-vis spectra. Anal Chem 2007;79:4215–21.

51. Chithrani BD, Ghazani AA, Chan WCW. Determining the size and shape dependence of gold nanoparticle uptake into mammalian cells. Nano Lett 2006;6:662–8.

52. Pereira-Lachataignerais J, Pons R, Panizza P, et al. Study and formation of vesicle systems with low polydispersity index by ultrasound method. Chem Phys Lipids 2006;140:88–97.

53. Moraes CM, De Paula E, Rosa AH, Fraceto LF. Physicochemical stability of poly(lactide-co-glycolide) nanocapsules containing the local anesthetic bupivacaine. J Braz Chem Soc 2010;21:995–1000.

54. Aghajani M, Shahverdi AR, Amani A. The use of artificial neural networks for optimizing polydispersity index (PDI) in

nanoprecipitation process of acetaminophen in microfluidic devices. AAPS PharmSciTech 2012;13:1293–301.

55. Lewis G, Li Y. Dependence of in vitro fatigue properties of PMMA bone cement on the polydispersity index of its powder. J Mech Behav Biomed Mater 2010;3:94–101.

56. Rosenfeld C, Serra C, Brochon C, Hadziioannou G. Influence of micromixer characteristics on polydispersity index of block copolymers synthesized in continuous flow microreactors. Lab Chip 2008;8:1682–7.

57. Vieville J, Tanty M, Delsuc MA. Polydispersity index of polymers revealed by DOSY NMR. J Magn Reson 2011;212: 169–73.

58. Kaufman ED, Belyea J, Johnson MC, et al. Probing protein adsorption onto mercaptoundecanoic acid stabilized gold nanoparticles and surfaces by quartz crystal microbalance and zeta-potential measurements. Langmuir 2007;23:6053–62.

59. Santander-Ortega MJ, Jodar-Reyes AB, Csaba N, et al. Colloidal stability of pluronic F68-coated PLGA nanoparticles: a variety of stabilisation mechanisms. J Colloid Interface Sci 2006;302:522–9.

60. Parab HJ, Huang JH, Lai TC, et al. Biocompatible transferrin-conjugated sodium hexametaphosphate-stabilized gold nanoparticles: synthesis, characterization, cytotoxicity and cellular uptake. Nanotechnology 2011;22:395706.

61. Wang G, Sun W. Optical limiting of gold nanoparticle aggregates induced by electrolytes. J Phys Chem B 2006;110: 20901–5.

62. Aryal S, Remant BK, Narayan B, et al. Study of electrolyte induced aggregation of gold nanoparticles capped by amino acids. J Colloid Interface Sci 2006;299:191–7.

63. Aili D, Enander K, Rydberg J, et al. Aggregation-induced folding of a de novo designed polypeptide immobilized on gold nanoparticles. J Am Chem Soc 2006;128:2194–5.

64. Lee SH, Zhang ZP, Feng SS. Nanoparticles of poly(lactide)-tocopheryl polyethylene glycol succinate (PLA-TPGS) copolymers for protein drug delivery. Biomaterials 2007;28:2041–50.

65. Nishio K, Gokon N, Hasegawa M, et al. Identification of a chemical substructure that is immobilized to ferrite nanoparticles (FP). Colloids Surf B Biointerfaces 2007;54:249–53.